physica status solidi a

www.pss-a.com

applications and materials science

Effect of deep-level states on current–voltage characteristics and electroluminescence of blue and UV light-emitting diodes

R. Nana[1,2], **P. Gnanachchelvi**[1], **M. A. Awaah**[1], **M. H. Gowda**[1,3], **A. M. Kamto**[1,4], **Y. Wang**[5], **M. Park**[5], **and K. Das**[*,1]

[1] Department of Electrical Engineering, Tuskegee University, Tuskegee, AL 36088, USA
[2] Present address: ViewRay Incorporated, 2 Thermo Fisher Way, Oakwood Village, OH 44146, USA
[3] Present address: Department of Computer Science and Engineering, T. John Institute of Technology, Bangalore 560023, India
[4] Present address: Department of Electrical and Computer Engineering, The University of Alabama, Tuscaloosa, AL 35487, USA
[5] Department of Physics, Auburn University, Auburn, AL 36849, USA

* Corresponding author: e-mail dask@tuskegee.edu, Phone: 334 727 8994, Fax: 334 724 4806.

Current–voltage (I–V) characteristics and electroluminescence spectra of several ultraviolet and blue light-emitting diodes (LEDs) emitting nominally at 380, 400, 430, and 468 nm were studied. These diodes exhibited an Ohmic regime at low forward biases; then the current increased sharply as bias increased. Several changes in the slope of logarithmic I–V plots indicated that, $I \propto V^x$. These changes in the slope were interpreted as single-carrier space-charge-limited (SCL) transport across the diode active region. As bias increased the deep states were filled and for the 400- and 468-nm diodes ideality factors of ~2 were obtained. This indicated that, as bias increased the transport mechanism changed from SCL conduction to recombination of injected carriers in the space-charge region. For the 380- and 430-nm diodes, ideality factors >>2 were obtained, although the observed electroluminescence spectrum indicated substantial radiative recombination. For the diode emitting at 430 nm, several peaks including the major peak at ~424 nm appeared to have resulted from transitions between the conduction-band edge and deep states, identified from the I–V characteristics, likely to be associated with Zn doping of the InGaN active region. Deep states in the other diodes appeared to be ineffective in the radiative recombination process.

© 2010 WILEY-VCH Verlag GmbH & Co. KGaA, Weinheim

1 Introduction Group-III nitride-based high-intensity blue light-emitting diodes (LEDs) have been available commercially for a number of years. Ultraviolet LEDs have also been introduced recently. These light sources are finding a wide range of applications, and are beginning to be employed for general illumination. A chronological account of the development of these relatively new classes of LEDs has been given by Schubert in an excellent text on LEDs [1]. Growth and properties of III-nitride thin films and fabrication of LEDs and laser diodes have been considered in detail by Nakamura et al. in "The Blue Laser Diode – The Complete Story" [2].

Large GaN substrates are not yet available commercially, thin films are grown heteroepitaxially, commonly on sapphire and 6H-SiC substrates. Silicon carbide provides a better lattice match with GaN. Due to the mismatch, grown films have a high density of crystallographic defects. These defects have been reported to be benign and do not affect high-intensity light emission [3]. However, some research groups report improvement in emission intensity in films with reduced defect density [4]. This observation indicates the defects have some deleterious effect on optical performance of III-nitride diodes through nonradiative processes. A strong connection between the high intrinsic defect density in these devices and the resulting mode of degradation has also been observed [5]. Nonradiative processes are likely to occur through the participation of deep-states generated by crystallographic defects and/or impurities present in the films. The presence of defects in the LED active region, are also likely to affect diode electrical

characteristics. However, crystalline defects, their role in creating radiatively active/inactive deep states and effects on LED *I–V* characteristics and emission spectra are not well understood at this stage.

The current in a *p–n* junction diode is normally given by

$$I = I_s \exp(qV/\mathrm{n}kT),$$

where *n*, the ideality factor is 1 for an ideal diode where recombination in the space-charge region of the diode is negligible and 2 for a diode where recombination in the space-charge region dominates the diode current.

LEDs being recombination-dominated devices, it is expected that the ideality factor should be 2. In commercially available red and yellow LEDs an ideality factor of ∼2 is commonly observed, infrared LEDs show an ideality of ∼2 at low biases, and ∼1.7 at high biases. However, in the early stages of development, blue and ultraviolet LEDs exhibited ideality factors >>2.

Shah et al. [6] proposed a model to account for the high ideality factor observed in their GaN *p–n* junctions and *p–n* junction structures with a p-type AlGaN/GaN superlattice that facilitates the formation of low-resistance Ohmic contacts. Their model considers two additional rectifying junctions; one arising from an AlGaN/GaN heterojunction and the other from a metal-p-type semiconductor contact, both with parallel resistors. The metal–semiconductor rectifying contact was considered to have a reversed polarity. The complete equivalent circuit also considered a resistance in series with the combination of the three junctions.

Several research groups considered the high ideality factors to be due to deep-level-assisted tunneling [7–10]. However, some other researchers reported that the *I–V* relationship in GaN *p–i–n* diodes and AlGaN/GaN based LEDs followed a power-law-type relationship given by, $I \propto V^x$ [11–13]. At low biases, $x = 1$, indicating Ohmic conduction; at higher biases current rose sharply giving higher values of *x*. It was inferred from these observations that conduction in these diodes was due to space-charge-limited (SCL) transport in the presence of traps [14, 15]. Determination of approximate concentrations of trap states and their location in the bandgap were also obtained from an analysis of the SCL *I–V* characteristics [16]. It should be noted that traps are essentially deep states located closer to the conduction or the valence-band edge as opposed to midgap states that act as efficient recombination centers [17].

In some recent studies of GaN/InGaN/GaN MQW structures, ideality factors $1 < n < 2$ (a combination of diffusion in the quasineutral and recombination in the space-charge regions) have been observed; these are attributed to higher material quality than that used in previous studies [9, 18–20]. However, at biases below turn-on, in most cases excess currents are observed that cannot be meaningfully described by the exponential diode equation. It appears that these *I–V* characteristics at low biases can be better described by power-law relationships that would be expected for SCL transport of carriers in the presence of deep-level states.

In this paper, we report a study of *I–V* characteristics and electroluminescence spectra of several commercially obtained blue and ultraviolet LEDs. Effects of SCL transport, recombination in the space-charge region and series resistance have been considered in determining the *I–V* relationship of these LEDs. The effect of deep-level states, as determined from the SCL current analysis, on the electroluminescence spectra are also highlighted. In some cases, the electroluminescence spectra indicated that the deep level states were active in the process of radiative recombination.

2 Space-charge-limited current (SCLC) SCLC in insulators has been considered in detail by Lampert and Mark [14]. They loosely define materials with a bandgap above 2 eV as insulators. Since group-III nitride-based semiconductors, such as AlGaN/InGaN/GaN structures have bandgaps >2 eV, using Lampert and Mark's criterion, these may be considered as insulators. For the sake of completeness we summarize here a phenomenological description of SCLC in insulators, as given by Rose [15], and Lampert and Mark [14].

Current density, *J*, in an ideal insulator that is free from any trapping states, is characterized by its square law dependence on voltage, *V*,

$$J \propto V^2.$$

An approximate expression for SCL current given by,

$$J \sim \varepsilon \varepsilon_0 \mu \left(V^2/L^3\right), \tag{1}$$

can be derived, using the approach employed by Rose, and Lampert and Mark, starting from, $Q = CV$, and defining current density as, $J = Q/t$, then using, $C = \varepsilon \varepsilon_0 / L$, $t = L/v$, $v = \mu E$, and $E = V/L$, where *Q* is the charge in the insulator, *t* the transit time, *ε* the relative dielectric constant, ε_0 the permittivity of free space, *L* the thickness of the insulator, *v* the drift velocity, and *μ* is the low-field mobility. An exact expression for the SCL current will have a numerical factor of 9/8 [14].

However, a real insulator is expected to have trapping states arising from defects and also a thermally generated free carrier concentration, n_0, arising from shallow dopants (similar to P or As donors in Si). At low voltages, the free-carrier concentration will contribute to an Ohmic conduction given by,

$$J = \varepsilon n_0 \mu (V/L). \tag{2}$$

At any voltage, *V*, there will be another component of charge in the insulator given by, $Q = CV$. At low voltages, carriers constituting this injected-charge effect will not have any significant effect on the Ohmic conduction. However, when the injected charge concentration exceeds n_0, space-charge effects set in and in a trap-free insulator, a transition

from Ohmic to, $J \propto V^2$, regime will occur at a voltage given by

$$V_x = qn_0L^2 / \varepsilon\varepsilon_0. \tag{3}$$

In insulators where carrier trap states are present, the V^2 regime will occur only when unoccupied trap states are filled with captured injected carriers. When all the trap states are filled, there will be a sharp transition in current from an Ohmic to the square-law regime, as shown schematically in Figs. 1a and b.

Lampert and Mark distinguish between shallow and deep traps depending on their position in the bandgap. They term those located above the Fermi level (quasi-Fermi level to be more precise) as "shallow" traps and those at or below the (quasi-)Fermi level as "deep" traps. These shallow states are considered to be much deeper than the shallow donor states. The detailed nature of the I–V characteristics depends on whether the traps are shallow or deep, as indicated in Figs. 1c and d.

2.1 Shallow traps For shallow traps, such that $(E_t > E_f)$, the quasi-Fermi level, E_f, corresponds to the free-electron concentration,

$$n = n_i + n_0.$$

where n_i is the injected carrier concentration. If the ratio, θ, of the total free electron concentration, n, to the trapped state concentration, n_t, is given as,

$\theta = $ (injected + thermal equilibrium concentration)/ trapped state concentration $\ll 1$, current can be given as

$$J = \theta\varepsilon\varepsilon_0\mu\left(V^2/L^3\right). \tag{4}$$

Transition from the Ohmic to the shallow-trap square-law-regime will occur at $1/\theta$ of voltage, V_x,

$$V_{x\theta} = qn_0L^2 / \theta\varepsilon\varepsilon_0, \tag{5}$$

as indicated in Fig. 1c.

2.2 Deep traps In the presence of deep-trap states, such that $(E_f > E_t)$, Ohmic conduction will be obtained to a voltage V_x, when the injected free-electron concentration, n_i becomes comparable to the thermal equilibrium concentration n_0. At this point it is considered that a doubling of the injected free-carrier concentration will fill all the traps due to an upward swing of the quasi-Fermi level. In this case, V_x coincides with filling of the traps, contributing to a charge $Q(V_{TFL}) = qp_{t_0}L$; since all traps are filled, this voltage is referred to as the trap-filled-limit, V_{TFL}, given by

$$V_{TFL} = qp_{t_0}L^2 / \varepsilon\varepsilon_0, \tag{6}$$

where p_{t_0} is the density of unoccupied traps, alternatively traps occupied by holes. A schematic of the I–V characteristics expected in this case is shown in Fig. 1d.

The current at a voltage higher than V_{TFL}, can be estimated by considering that a doubling of the voltage will effectively double the charge (trapped charge + mobile carriers). The ratio of current at $2V_{TFL}$ to current at V_{TFL} can be given approximately as

$$J(2V_{TFL})/J(V_{TFL}) \sim p_{t_0}/n_0; \tag{7}$$

p_{t_0} may be determined from the experimentally determined V_{TFL}, and n_0, from the observed $J(2V_{TFL})/J(V_{TFL})$ ratio. From the calculated value of n_0, the effective Fermi level, E_f (the quasi-Fermi level), can be calculated from

$$n_0 = N_c \exp[-(E_c - E_f)/kT]. \tag{8}$$

E_f is considered to be the approximate position of the deep-trap state and p_{t_0} is the corresponding concentration of unoccupied states at this level [14]. For p-type material, n_0 will be replaced by p_0, N_c by N_v, and $(E_c$–$E_f)$ by $(E_f$–$E_v)$; also shallow traps will be located below and deep traps above the quasi-Fermi level. However, the above approach cannot specify whether the trap states are located close to the conduction or the valence-band edge. In the present study, it
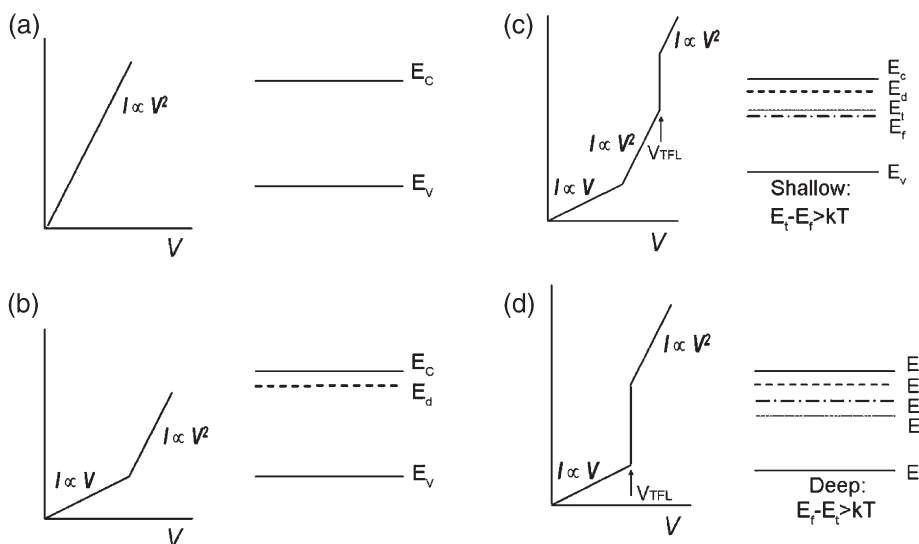

Figure 1 SCLC I–V characteristics. (a) Ideal insulator, (b) insulator with thermally generated carriers, (c) insulator with "shallow" traps, and (d) insulator with "deep" traps.

was inferred that the deep-trap states were located close to the valence-band edge as the active region of the LEDs were most likely p-type doped with Zn [2]. This inference was also supported by the observation that certain emission peaks in the electroluminescence spectra, appeared to occur due to transitions from the conduction-band edge to deep trapping states close to the valence band, *i.e.*, $h\nu = E_c - (E_v + E_t)$.

3 Experimental Commercially available LEDs with major emission peaks occurring at 380, 400, 430, and 468 nm, were used in this study.

I–V measurements were obtained using a HP 4155A semiconductor parameter analyzer (SPA). Linear, semilogarithmic (forward current) and logarithmic (forward current) plots of *I–V* characteristics were obtained. For all electrical measurements the LEDs were placed in a metal shielded box.

For the linear plots the LEDs were driven from a reverse bias of −20 V to a forward bias of 5 V at steps of 0.01 V. The medium integration option on the SPA was employed for all *I–V* measurements.

For the semilogarithmic and logarithmic plots the diodes were driven from zero bias to a forward bias of 5 V at steps of 0.025 V. Plots were recorded from a current level of 1×10^{-12} A to 100 mA. The limit of sensitivity of the SPA 4155A is $\sim 1 \times 10^{-12}$ A, however, in some cases currents below, 1×10^{-12} A, were also recorded in order to visualize the power-law trend of the *I–V* curves at low current levels.

Capacitance–voltage (*C–V*) measurements were obtained for zero bias using an HP 4284A LCR meter at a frequency of 1 MHz. Depletion widths determined from the measured capacitances were used as the active region thickness in the calculation of deep-level trap parameters.

Optical emission (electroluminescence) spectra from the LEDs were collected using a Jobin-Yvon TRIAX 550 spectrometer equipped with a thermoelectrically cooled charge coupled device (CCD) detector. Spectra were obtained for drive currents of 10, 20 mA, and then at 20 mA intervals until the diodes failed. The minimum voltage/current at which detectable light emission occurred was also noted for each LED.

4 Results On visual inspection of the LEDs, it appeared that these were vertically contacted devices. Vertically contacted devices normally employ highly conducting SiC substrates for heteroepitaxial growth of the III-nitride device layers. These LED devices generally have a double heterojunction structure of the type-p-GaN/p-$Al_xGa_{1-x}N$/p-$In_xGa_{1-x}N$/n-$Al_xGa_{1-x}N$/n-GaN/n-6H SiC, as shown schematically in Fig. 2 [21, 22]. In the devices discussed in Refs. [21, 22] the AlGaN layers had a compositon of $Al_{0.1}Ga_{0.9}N$. A similar structure has also been employed for the fabrication of laterally contacted InGaN LEDs on sapphire substrates [2]. The In/Ga ratio in the active $In_xGa_{1-x}N$ layer is determined by the required bandgap (color of emitted light). In the present study, the depletion width associated with the zero-bias junction
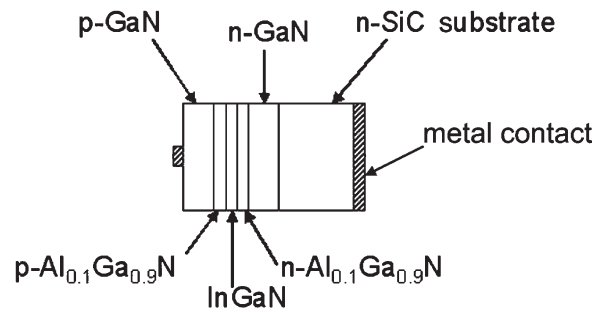

Figure 2 Schematic of the double heterojunction LED structure.

capacitance was taken as the approximate thickness of the active $In_xGa_{1-x}N$ region.

4.1 *I–V* characteristics Linear plots of the *I–V* characteristics of these LEDs, showed a reasonably sharp forward turn-on and soft reverse breakdown. The 430-nm diode appeared to be the most resistive. Forward voltages for 20 mA of drive current were noted for each diode, as given in Table 1.

Semilogarithmic plots of the forward and reverse characteristics are shown in Fig. 3; three apparently linear regimes, delineated as n1, n2, and n3 were observed in these plots for forward currents ranging from $\sim 1 \times 10^{-12}$ to 0.1 A. The uppermost regime, n3 was used for the calculation of ideality factors, as given in Table 1. The range of voltage over which n3 occurs is comparable to that used by other researchers in calculating ideality factors for blue LEDs [7–10, 18–20].

LEDs emitting at 380 and 430 nm exhibited ideality factors >>2, whereas 400- and 468-nm LEDs yielded ideality factors of ~2. An ideality of 2 indicates that diode current is dominated by recombination in the space-charge region. However, the linearity of the n3 regime was observed over slightly more than one decade of current, the 430-nm diode showed linearity over less than one decade. In contrast, Shah et al. [6] observed linearity extending over five decades of current in their GaN *p–n* junctions, although their ideality factors were >>2.

Observed currents beyond regime n3 were totally controlled by series resistance in all the diodes studied. Series resistance values, as given in Table 1, were extracted from the observed deviation of the experimental *I–V* curve

Table 1 Optical "turn-on" voltage, V_{OTO} (voltage corresponding detectable emission), forward voltage for 20 mA of drive current, series resistance, ideality factor, and the range of voltage where linearity was observed (in parenthesis).

LED (nm)	V_{OTO} (V)	V_f at 20 mA (V)	R_s (Ω)	n3 (voltage range (V))
380	3.19	3.65	7.63	4.51 (2.8 < V < 3.35)
400	2.74	3.27	5.19	2.05 (2.8 < V < 3.05)
430	2.98	3.90	13.63	4.94 (3.1 < V < 3.55)
468	2.47	3.07	7.29	2 (2.4 < V < 2.7)

Original

Paper

Phys. Status Solidi A **207**, No. 6 (2010)   1493
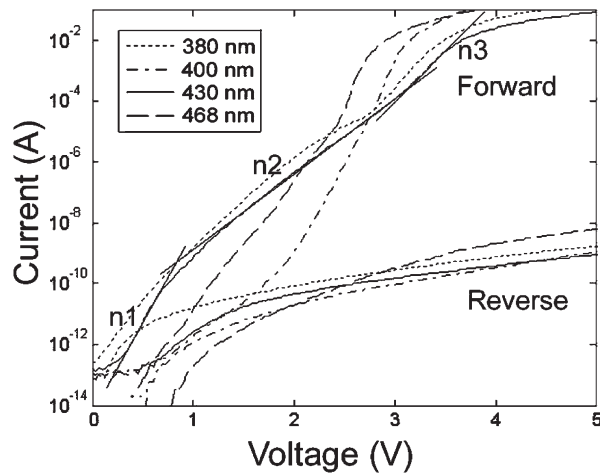
Figure 3 Semilogarithmic plots of LED forward and reverse characteristics. Three linear regimes designated as n1, n2, and n3 are indicated. Ideality factors were calculated from regime n3. Detectable electroluminescence was observed as the LEDs entered regime n3.

Figure 4 Logarithmic plots of LED forward characteristics. Various power-law regimes and V_{TFL}s, where sharp rise in current is observed for the 430-nm LED, are shown in the inset. The LED emitting at 380 nm also exhibits an ($I \propto V^2$) regime for low biases.

from the slope of regime n3 in the semilogarithmic plots. The slopes of the experimental *I–V* curves at lower biases, since currents were low, did not show any appreciable change when diode voltages were adjusted to take the series resistance into consideration.

Ideality factors calculated for currents at lower and intermediate biases, regimes n1 and n2, were generally $>>2$ in all cases. It was inferred that low diode currents cannot be meaningfully described by an exponential relationship with a given value of the ideality factor. As detailed in the following section, currents at low biases for all diodes and also at high biases for the 380- and 430-nm diodes have been interpreted as SCL in the presence of high concentrations of trapping states.

Logarithmic plots of the forward characteristics, as shown in Fig. 4, for all the LEDs appear to have several power-law regimes given by, $I \propto V^x$, where x exhibits a number of different values. Values of x and the corresponding range of voltages are given in Table 2. At very low biases, $x = 1$ or ($I \propto V$), indicating Ohmic conduction. The Ohmic conduction does not appear to be due to surface leakage; in the case of surface leakage a symmetrical Ohmic conduction would be expected for both forward and reverse polarities [23]. Observed reverse currents in these LEDs at low biases were non-Ohmic and much lower than forward currents (Fig. 3).
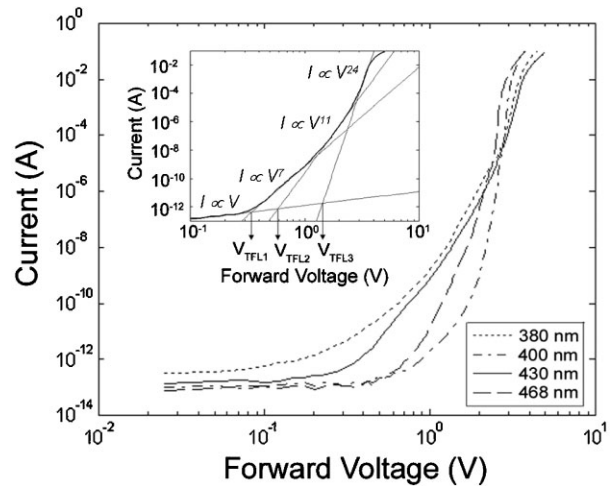
For higher biases x increased sharply. These voltage dependences appear to be what would be expected for SCLC flow in insulators contributed by single-carrier injection. As considered by Casey et al. [7], it is likely that carriers (holes) enter the active region at biases much lower than the built-in potential by tunneling from the p-type AlGaN layer into localized deep states within the bandgap of the InGaN active layer. It is speculated here that these carriers, once into the active region are subjected to SCL transport influenced by deep trapping states.

Concentration of injected carriers increases with increasing bias and each change in slope in the *I–V*, as seen in the logarithmic plots, corresponds to capture of injected carriers and consequent full occupation of deep traps at a certain level. The voltage, at which Ohmic conduction to sharp rise in current occurs, is designated as V_{TFL1}. Subsequent changes in the slope of the *I–V* curve, as indicated in Fig. 4, are considered to be due to the presence of more than one set of trapping centers. Voltages, at which these changes occur, are designated by V_{TFL2} and V_{TFL3}. The observed slope of 2 ($I \propto V^2$) for the 380-nm diode immediately following the Ohmic regime is due to the presence of "shallow traps" located below the quasi-Fermi level in the p-type active region. It should be noted that these shallow traps are much deeper than normal donor or acceptor states. Densities of deep trapping centers and their positions

Table 2 Power-law regimes and voltage ranges for each power-law regime (in parenthesis) observed in the LED forward characteristics.

LED (nm)	380	400	430	468
regime 1	$I \propto V$ ($0.06 \leq V \leq 0.14$)	$I \propto V$ ($0.28 \leq V \leq 0.72$)	$I \propto V$ ($0.10 \leq V \leq 0.35$)	$I \propto V$ ($0.31 \leq V \leq 0.56$)
regime 2	$I \propto V^2$ ($0.14 \leq V \leq 0.35$)	$I \propto V^6$ ($0.72 \leq V \leq 1.90$)	$I \propto V^7$ ($0.35 \leq V \leq 1.30$)	$I \propto V^{13}$ ($0.56 \leq V \leq 1.70$)
regime 3	$I \propto V^5$ ($0.35 \leq V \leq 1.02$)	$I \propto V^{34}$ ($1.90 \leq V \leq 2.66$)	$I \propto V^{11}$ ($1.30 \leq V \leq 2.85$)	$I \propto V^{22}$ ($1.70 \leq V \leq 2.42$)
regime 4	$I \propto V^{11}$ ($1.02 \leq V \leq 2.80$)	$I \propto V^{48}$ ($2.66 \leq V \leq 3.10$)	$I \propto V^{24}$ ($2.85 \leq V \leq 3.70$)	$I \propto V^{48}$ ($2.42 \leq V \leq 2.68$)
regime 5	$I \propto V^{25}$ ($2.80 \leq V \leq 3.42$)			

Table 3 V_{TFL} values from logarithmic plots, concentration of occupied traps, n_{t_0}, effective hole concentration in the active region, p_0 (active region considered to be highly compensated or p-type), trap level E_t.

LED (nm)	V_{TFL}	n_{t_0} (cm^{-3})	p_0 (cm^{-3})	E_t–E_v (eV)
380	0.27	2.63×10^{16}	7.89×10^{14}	0.26
	0.60	5.84×10^{16}	3.15×10^{13}	0.34
	1.48	1.44×10^{17}	4.61×10^{9}	0.57
400	0.75	2.66×10^{16}	3.78×10^{14}	0.28
	1.64	5.81×10^{16}	2.18×10^{6}	0.77
	1.90	6.73×10^{16}	5.72×10^{5}	0.80
430	0.35	4.35×10^{16}	2.84×10^{14}	0.29
	0.59	7.34×10^{16}	1.71×10^{13}	0.36
	1.43	1.78×10^{17}	5.50×10^{9}	0.57
468	0.75	2.86×10^{17}	2.86×10^{13}	0.35
	1.07	4.08×10^{17}	1.30×10^{11}	0.49
	1.68	6.41×10^{17}	7.66×10^{6}	0.74

Table 4 Electroluminescence spectra – summary of observations: peak positions at low and high drive currents, and radiative transitions.

LED (nm)	peak position at low I_f (nm)	peak position at high I_f (nm)	radiative transition
380	381	395	E_c–E_v
	392 (shoulder)	-	E_c–$(E_v + 0.10\,\text{eV})$
400	399	420	E_c–E_v
430	-	380	E_c–E_v
	407 (shoulder)	407	E_c–$(E_v + 0.21\,\text{eV})$
	424 (major peak)	424	E_c–$(E_v + 0.34\,\text{eV})$
	453 (shoulder)	453	E_c–$(E_v + 0.52\,\text{eV})$
468	459	459	E_c–E_v

in the bandgap were calculated, from the observed V_{TFL}s, using Eqs. (6)–(8), are given in Table 3. For the 430-nm LED, in particular, three different deep trap levels located at 0.29, 0.36, and 0.57 eV (above the valence-band edge, as inferred from the electroluminescence spectra) and with concentrations of 4.35×10^{16}, 7.34×10^{16}, and $1.78 \times 10^{17}\,\text{cm}^{-3}$ were observed, respectively. For the calculation of the trap levels an N_v of $1.8 \times 10^{19}\,\text{cm}^{-3}$ was used [1].

When all the trapping states become occupied with increasing bias, the transport mechanism appears to change. For the 400- and 468-nm diodes, at biases of 2.8 and 2.4 V, respectively, the diodes enter a space-charge-region-recombination-dominated current regime (n3), where injected electrons and holes recombine radiatively, contributing to detectable light emission. This recombination dominated current regime is characterized by an ideality factor of ~2, as obtained from the regime n3 in the semilogarithmic plots. The 380- and 430-nm diodes do not yield ideality factors of 2; although substantial radiative recombination takes place when the diodes enter the n3 regime. It is probable that in these diodes, current is still determined in part by trap filling.

4.2 Electroluminescence spectra Electroluminescence spectra obtained from the LEDs as a function of drive current are shown in Fig. 5, and the observations are summarized in Table 4. The 380-nm LED showed a major peak at ~381 nm and a shoulder at 392 nm, for a drive current of 10 mA. The major peak at 381 nm gradually shifted to longer wavelengths with increasing drive currents, reaching ~395 nm for 100 mA. However, the shoulder could not be discerned from the major peak at high drive currents. The 400-nm LED had a single peak at ~399 nm for a drive current of 10 mA, shifting to ~420 nm for 80 mA. This shift in the peak positions for the 380- and the 400-nm LEDs is probably due to bandgap narrowing due to a rise in junction temperature at higher drive currents [1]. For the 430-nm LED, the major peak occurred at ~424 nm, and shoulders

were observed at 407 nm and at 453 nm. An additional peak at ~380 nm appeared at high drive currents. The 468-nm LED had a single peak at 459 nm. The emission peaks in the 430- and 468-nm LEDs did not show any shift in the peak position with increase in drive currents. However, a broadening of the peaks was observed with increasing currents in all the LEDs.

4.3 Radiative recombination through trap states Although electrically active traps were identified in all the devices studied here, only one shallow trap in the 380-nm LED and several deep traps in the 430-nm LED appear to be active in the radiative recombination process. For the 380-nm LED the shoulder at 392 nm corresponds to a transition energy of 3.16 eV. Assuming that the 380 nm peak is the band-edge emission corresponding to a bandgap of 3.26 eV, the shoulder at 392 nm appears to be due to a transition from the conduction-band edge to a state located at 0.10 eV above the valence-band edge; $[(E_t–E_v) = (3.26–3.16\,\text{eV}) = 0.10\,\text{eV}]$. This radiatively active trap state appears to act as a shallow trap yielding the, $I \propto V^2$, regime in the logarithmic plot of the I–V characteristics for the 380-nm diode (Fig. 4).

For the 430-nm diode, the observed (for high drive currents) peak at 380 nm appears to correspond to a band-edge emission for an energy gap of 3.26 eV. A band-edge emission around 380 nm was also observed by Osinski et al. [5] at high (pulsed) current levels in AlGaN/InGaN/GaN diodes. Assuming that the present LED had a structure similar to that studied by Osinski et al., the peaks occurring at 407 (minor peak), 424 (major peak), and 453 nm (minor peak) appear to be due to transitions from the conduction-band minimum to deep trapping states located at 0.21, 0.34, and 0.52 eV above the valence-band edge, respectively. From Table 3, it can be seen that the deep levels as determined from the SCL current analysis (0.29, 0.36, and 0.57 eV) are in reasonably close agreement with those corresponding to peak positions in the electroluminescence spectra. Thus, it is inferred that electrically active deep
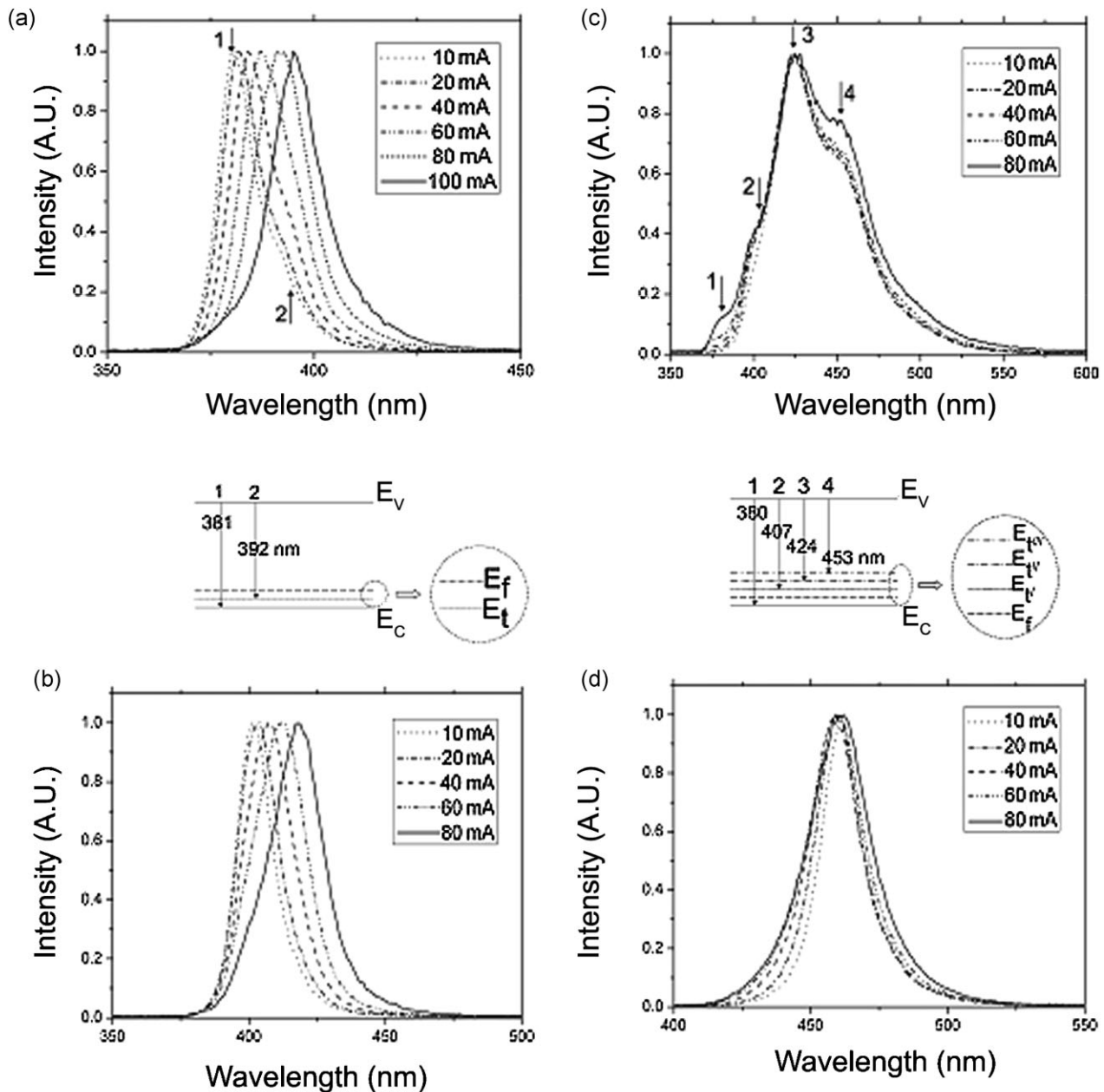
Original

Paper

Phys. Status Solidi A **207**, No. 6 (2010)   1495

Figure 5 Normalized electroluminescence spectra obtained from the LEDs with increasing drive current. A broadening of peaks were observed for all LEDs with increasing drive current. (a) LED emitting at 380 nm. The major peak occurring at 381 nm, appears to be the bandgap radiation and the shoulder at 392 nm appears to be due to a transition to a state located 0.10 eV above the valence band. These radiative transitions occurring in this LED are indicated schematically in the accompanied band diagram. The shift in the position of the major peak is probably due to bandgap narrowing arising from rise in temperature as drive current increases. The shoulder at 392 nm observed at low currents is not discernible at high drive currents. (b) LED emitting at 400 nm. The shift in peak position is similar to that observed for the 380-nm LED. (c) LED emitting at 430 nm. At low drive currents two shoulders, one at a shorter (407 nm) and the other at a wavelength longer (453 nm) than the major peak (424 nm), are observed. At a higher drive current a shoulder at 380 nm is also observed, however, no shift in peak position was observed at high currents. The 380-nm peak appears to be the bandedge emission for a material with a bandgap of 3.26 eV. Radiative transitions occurring in this LED are indicated schematically in the accompanied band diagram. The bandgap radiation (380 nm) is marked as "1", transition "2" (407 nm) is shown to arise from a transition to level $E_{t'}$ located at 0.21 eV + E_v, "3" (424 nm – major peak) from a transition to $E_{t''}$ at 0.34 eV + E_v, and "4" (453 nm) from a transition to $E_{t'''}$ at 0.52 eV + E_v. (d) LED emitting at 468 nm. A very small shift in peak position is observed as drive current is increased to 80 mA.

states in the 430-nm diode are also active in the process of radiative recombination. It is noted that levels between 0.4 and 0.5 eV above valence band are associated with Zn doping of the $In_xGa_{1-x}N$ active region [2].

The single-emission peaks observed in the 400- and 468-nm LEDs indicate that the peaks arise from a single probably band-edge transition in $In_xGa_{1-x}N$ with bandgaps of 3.10 eV (400 nm, $In_{0.12}Ga_{0.88}N$) and 2.65 eV (468 nm, $In_{0.15}Ga_{0.85}N$) [2]. The single-peak spectra also indicate that the deep-level trapping centers identified from the analysis of *I–V* plots are not active in the radiative recombination process.

5 Conclusions *I–V* characteristics of several commercially available ultraviolet and blue LEDs, emitting nominally at 380, 400, 430, and 468 nm, exhibited an Ohmic regime at very low forward biases. Subsequently, the current increased sharply at higher biases. Several changes in the slope of the logarithmic plots were also observed in the sharply rising current regime, indicating that $I \propto V^x$. These observed changes in the slope of the *I–V* plots, were interpreted as single-carrier SCL transport of carriers across the diode active region. Approximate concentration and position of the deep-level states in the bandgap were extracted from the voltage and current at which changes were observed in the slope of logarithmic plots of the *I–V* characteristics. For the LED emitting at 430 nm, the trap states are located at 0.29, 0.36, and 0.57 eV above the valence-band edge with concentration of 4.35×10^{16}, 7.34×10^{16}, and 1.78×10^{17} cm^{-3}, respectively. These deep states are most likely associated with Zn dopant in the InGaN active region and appear to be active in the radiative recombination process. For the 400- and 468-nm LEDs, however, the deep states obtained from the analysis of the *I–V* characteristics are not radiatively active. The 392 nm shoulder in the 380-nm diode spectrum appear to arise from a shallow trap state located at 0.10 eV above the band edge.

As bias increased, the deep traps in the 400- and 468-nm LEDs were completely filled, and current could be given by the diode equation with an ideality factor of ~2. An ideality factor of 2 indicated that recombination of injected electrons and holes in the space-charge region dominated current transport. The bias at which SCLC regime changed over to a recombination-dominated regime also coincided with "optical turn-on" of these LEDs. For the 380- and 430-nm devices, ideality factors >2 were obtained, indicating that the diode equation could not meaningfully describe the current in these diodes, although the observed electroluminescence spectrum indicated substantial radiative recombination. Eventually, current in all the diodes studied was controlled by series resistance.

References

[1] E. F. Schubert, Light–Emitting Diodes (Cambridge University Press, Cambridge, 2006).

[2] S. Nakamura, S. Pearton, and G. Fasol, The Blue Laser Diode – The Complete Story (Springer-Verlag, Berlin, 2000).

[3] S. D. Lester, F. A. Ponce, M. G. Craford, and D. A. Steigerwald, Appl. Phys. Lett. **66**, 1249 (1995).

[4] T. Miyajima, T. Hino, S. Tomiya, K. Yanashima, S. Hashimoto, T. Kobayashi, M. Ikeda, A. Satake, E. Tokunaga, and Y. Masumoto, Non-radiative nature of threading dislocations in GaN grown by metal-organic chemical vapor deposition, presented at the Int. Workshop on Nitride Semiconductors, Nagoya, Japan, 2000.

[5] M. Osinski, J. Zeller, P.-C. Chiu, and B. C. Phillips, Appl. Phys. Lett. **69**, 898 (1996).

[6] J. M. Shah, Y.-L. Li, T. Gessmann, and E. F. Schubert, J. Appl. Phys. **94**, 2627 (2003).

[7] H. C. Casey, Jr., J. Muth, S. Krishnakutty, and J. M. Zavada, Appl. Phys Lett. **68**, 2867 (1996).

[8] P. Perlin, M. Osinski, P. G. Eliseev, V. A. Smagley, J. Mu, M. Banas, and P. Sartori, Appl. Phys. Lett. **69**, 1680 (1996).

[9] A. Chitnis, A. Kumar, M. Shatalov, V. adiVarahan, A. Lunev, J. W. Yang, G. Simin, A. Asif Khan, R. Gaska, and M. Shur, Appl. Phys Lett. **77**, 3800 (2000).

[10] X. A. Cao, E. B. Stokes, P. M. Sandvik, S. F. LeBoeuf, J. Kretchmer, and D. Walker, IEEE Electron Devices Lett. **23**, 535 (2002).

[11] V. A. Dimitiev, MRS Internet J. Nitride Semicond. Res. **1**, Article 29 (1996).

[12] R. H. Khan, M. Kamruzzaman, S. L. Saha, K. Hiramatsu, and N. Sawaki, Electrical properties of electroluminescence of GaN:Mg blue light-emitting diodes, presented at the Int. Workshop on Physics of Semiconducting Devices, No. 9, Delhi, September 16–20, 1997.

[13] T. M. Williams, C. van Eyck, K. Das, D. B. Slater, and J. A. Edmond, Electrical characterization of GaN/AlGaN/GaN Double heterojunction blue light-emitting diodes, presented at the MRS Fall Meeting, paper D15.43, Boston, December 1–5, 1997.

[14] M. A. Lampert and P. Mark, Current Injection in Solids (Academic Press, New York, 1970).

[15] A. Rose, Phys. Rev. **97**, 1538 (1955).

[16] M. A. Awaah, R. Nana, and K. Das, Mater. Res. Soc. Symp. Proc. **829**, B2. 11. 1 (2005).

[17] B. G. Streetman and S. K. Banerjee, Solid State Electronic Devices (Pearson Prentice Hall, Upper Saddle River, NJ, 2006).

[18] J. K. Sheu, G. C. Chi, Y. K. Su, C. C. Liu, C. M. Chang, W. C. Hung, and M. J. Jou, Solid State Electron. **44**, 1055 (2000).

[19] L. C. Chen, J.-B. Huang, P.-J. Cheng, and L.-S. Hong, Semicond. Sci. Technol. **22**, 1178 (2007).

[20] C.-L. Wang, M.-C. Tsai, J.-R. Gong, W.-T. Liao, P.-Y. Lin, K.-Y. Yen, C.-C. Chang, H.-Y. Lin, and S.-K. Hwang, Mater. Sci. Eng., B **138**, 180 (2007).

[21] H.-S. Kong, Mater. Res. Soc. Symp. Proc. **395**, 903 (1996).

[22] S. P. Denbaars, Proc. IEEE **85**, 1740 (1997).

[23] L. Hirsch and A. S. Barriere, J. Appl. Phys. **94**, 5014 (2003).